Published for SISSA by Springer

Received: *August 6, 2013*
Accepted: *September 3, 2013*
Published: *October 1, 2013*

First evidence for the two-body charmless baryonic decay $B^0 \to p\bar{p}$

The LHCb collaboration

E-mail: eduardo.rodrigues@cern.ch

Abstract: The results of a search for the rare two-body charmless baryonic decays $B^0 \to p\bar{p}$ and $B_s^0 \to p\bar{p}$ are reported. The analysis uses a data sample, corresponding to an integrated luminosity of 0.9 fb^{-1}, of pp collision data collected by the LHCb experiment at a centre-of-mass energy of 7 TeV. An excess of $B^0 \to p\bar{p}$ candidates with respect to background expectations is seen with a statistical significance of 3.3 standard deviations. This is the first evidence for a two-body charmless baryonic B^0 decay. No significant $B_s^0 \to p\bar{p}$ signal is observed, leading to an improvement of three orders of magnitude over previous bounds. If the excess events are interpreted as signal, the 68.3% confidence level intervals on the branching fractions are

$$\mathcal{B}(B^0 \to p\bar{p}) = \left(1.47\,^{+0.62\,+0.35}_{-0.51\,-0.14}\right) \times 10^{-8}\,,$$
$$\mathcal{B}(B_s^0 \to p\bar{p}) = \left(2.84\,^{+2.03\,+0.85}_{-1.68\,-0.18}\right) \times 10^{-8}\,,$$

where the first uncertainty is statistical and the second is systematic.

Keywords: QCD, Branching fraction, B physics, Flavor physics, Hadron-Hadron Scattering

ArXiv ePrint: 1308.0961

doi:10.1007/JHEP10(2013)005

JHEP10(2013)005

Contents

JHEP10(2013)005

1 Introduction

The observation of B meson decays into two charmless mesons has been reported in several decay modes [1]. Despite various searches at e^+e^- colliders [2–5], it is only recently that the LHCb collaboration reported the first observation of a two-body charmless baryonic B decay, the $B^+ \to p\overline{\Lambda}(1520)$ mode [6]. This situation is in contrast with the observation of a multitude of three-body charmless baryonic B decays whose branching fractions are known to be larger than those of the two-body modes; the former exhibit a so-called threshold enhancement, with the baryon-antibaryon pair being preferentially produced at low invariant mass, while the suppression of the latter may be related to the same effect [7].

In this paper, a search for the $B^0 \to p\overline{p}$ and $B_s^0 \to p\overline{p}$ rare decay modes at LHCb is presented. Both branching fractions are measured with respect to that of the $B^0 \to K^+\pi^-$ decay mode. The inclusion of charge-conjugate processes is implied throughout this paper.

In the Standard Model (SM), the $B^0 \to p\overline{p}$ mode decays via the $b \to u$ tree-level process whereas the penguin-dominated decay $B_s^0 \to p\overline{p}$ is expected to be further suppressed. Theoretical predictions of the branching fractions for two-body charmless baryonic B^0 decays within the SM vary depending on the method of calculation used, e.g. quantum chromodynamics sum rules, diquark model and pole model. The predicted branching fractions are typically of order $10^{-7} - 10^{-6}$ [8–12]. No theoretical predictions have been published for the branching fraction of two-body charmless baryonic decays of the B_s^0 meson.

The experimental 90% confidence level (CL) upper limit on the $B^0 \to p\overline{p}$ branching fraction, $\mathcal{B}(B^0 \to p\overline{p}) < 1.1 \times 10^{-7}$, is dominated by the latest search by the Belle experiment [5] and has already ruled out most theoretical predictions. A single experimental search exists for the corresponding $B_s^0 \to p\overline{p}$ mode, performed by ALEPH, yielding the upper limit $\mathcal{B}(B_s^0 \to p\overline{p}) < 5.9 \times 10^{-5}$ at 90% CL [2].

2 Detector and trigger

The LHCb detector [13] is a single-arm forward spectrometer covering the pseudorapidity range $2 < \eta < 5$, designed for the study of particles containing b or c quarks. The detector includes a high-precision tracking system consisting of a silicon-strip vertex detector surrounding the pp interaction region, a large-area silicon-strip detector located upstream of a dipole magnet with a bending power of about 4 Tm, and three stations of silicon-strip detectors and straw drift tubes placed downstream. The combined tracking system provides momentum measurement with relative uncertainty that varies from 0.4% at 5 GeV/c to 0.6% at 100 GeV/c, and impact parameter (IP) resolution of 20 µm for tracks with high transverse momentum ($p_{\rm T}$). Charged hadrons are identified using two ring-imaging Cherenkov detectors [14]. Photon, electron and hadron candidates are identified by a calorimeter system consisting of scintillating-pad and preshower detectors, an electromagnetic calorimeter and a hadronic calorimeter. Muons are identified by a system composed of alternating layers of iron and multiwire proportional chambers [15]. The trigger [16] consists of a hardware stage, based on information from the calorimeter and muon systems, followed by a software stage, which applies a full event reconstruction.

Events are triggered and subsequently selected in a similar way for both $B^0_{(s)} \to p\overline{p}$ signal modes and the normalisation channel $B^0 \to K^+\pi^-$. The software trigger requires a two-track secondary vertex with a large sum of track $p_{\rm T}$ and significant displacement from the primary pp interaction vertices (PVs). At least one track should have $p_{\rm T} > 1.7\,{\rm GeV}/c$ and $\chi^2_{\rm IP}$ with respect to any primary interaction greater than 16, where $\chi^2_{\rm IP}$ is defined as the difference in χ^2 from the fit of a given PV reconstructed with and without the considered track. A multivariate algorithm [17] is used for the identification of secondary vertices consistent with the decay of a b hadron.

Simulated data samples are used for determining the relative detector and selection efficiencies between the signal and the normalisation modes: pp collisions are generated using Pythia 6.4 [18] with a specific LHCb configuration [19]; decays of hadronic particles are described by EvtGen [20], in which final state radiation is generated using Photos [21]; and the interaction of the generated particles with the detector and its response are implemented using the Geant4 toolkit [22, 23] as described in ref. [24].

3 Candidate selection

The selection requirements of both signal modes and the normalisation channel exploit the characteristic topology of two-body decays and their kinematics. All daughter tracks tend to have larger $p_{\rm T}$ compared to generic tracks from light-quark background owing to the high B mass, therefore a minimum $p_{\rm T}$ requirement is imposed for all daughter candidates. Furthermore, the two daughters form a secondary vertex (SV) displaced from the PV due to the relatively long B lifetime. The reconstructed B momentum vector points to its production vertex, the PV, which results in the B meson having a small IP with respect to the PV. This is in contrast with the daughters, which tend to have a large IP with respect to the PV as they originate from the SV, therefore a minimum $\chi^2_{\rm IP}$ with respect to the

JHEP10(2013)005

PVs is imposed on the daughters. The condition that the B candidate comes from the PV is further reinforced by requiring that the angle between the B candidate momentum vector and the line joining the associated PV and the B decay vertex (B direction angle) is close to zero.

To avoid potential biases, $p\overline{p}$ candidates with invariant mass within $\pm 50\,\mathrm{MeV}/c^2$ ($\approx 3\sigma$) around the known B^0 and B_s^0 masses, specifically the region $[5230, 5417]\,\mathrm{MeV}/c^2$, are not examined until all analysis choices are finalised. The final selection of $p\overline{p}$ candidates relies on a boosted decision tree (BDT) algorithm [25] as a multivariate classifier to separate signal from background. Additional preselection criteria are applied prior to the BDT training.

The BDT is trained with simulated signal samples and data from the sidebands of the $p\overline{p}$ mass distribution as background. Of the $1.0\,\mathrm{fb}^{-1}$ of data recorded in 2011, 10% of the sample is exploited for the training of the $B^0_{(s)} \to p\overline{p}$ selection, and 90% for the actual search. The BDT training relies on an accurate description of the distributions of the selection variables in simulated events. The agreement between simulation and data is checked on the $B^0 \to K^+\pi^-$ proxy decay with distributions obtained from data using the *sPlot* technique [26]. No significant deviations are found, giving confidence that the inputs to the BDT yield a nearly optimal selection. The variables used in the BDT classifier are properties of the B candidate and of the B daughters, i.e. the proton and the antiproton. The B candidate variables are: the vertex χ^2 per number of degrees of freedom; the vertex χ^2_{IP}; the direction angle; the distance in z (the direction of the interacting proton beams) between its decay vertex and the related PV; and the p_{T} asymmetry within a cone around the B direction defined by $A_{p_{\mathrm{T}}} = ({p_{\mathrm{T}}}^B - {p_{\mathrm{T}}}^{\mathrm{cone}})/({p_{\mathrm{T}}}^B + {p_{\mathrm{T}}}^{\mathrm{cone}})$, with ${p_{\mathrm{T}}}^{\mathrm{cone}}$ being the p_{T} of the vector sum of the momenta of all tracks measured within the cone radius $R = 0.6$ around the B direction, except for the B-daughter particles. The cone radius is defined in pseudorapidity and azimuthal angle (η, ϕ) as $R = \sqrt{(\Delta\eta)^2 + (\Delta\phi)^2}$. The BDT selection variables on the daughters are: their distance of closest approach; the minimum of their p_{T}; the sum of their p_{T}; the minimum of their χ^2_{IP}; the maximum of their χ^2_{IP}; and the minimum of their cone multiplicities within the cone of radius $R = 0.6$ around them, the daughter cone multiplicity being calculated as the number of charged particles within the cone around each B daughter.

The cone-related discriminators are motivated as isolation variables. The cone multiplicity requirement ensures that the B daughters are reasonably isolated in space. The $A_{p_{\mathrm{T}}}$ requirement further exploits the isolation of signal daughters in comparison to random combinations of particles.

The figure of merit suggested in ref. [27] is used to determine the optimal selection point of the BDT classifier

$$\mathrm{FoM} = \frac{\epsilon^{\mathrm{BDT}}}{a/2 + \sqrt{B_{\mathrm{BDT}}}}\,, \tag{3.1}$$

where ϵ^{BDT} is the efficiency of the BDT selection on the $B^0_{(s)} \to p\overline{p}$ signal candidates, which is determined from simulation, B_{BDT} is the expected number of background events within the (initially excluded) signal region, estimated from the data sidebands, and the term $a = 3$ quantifies the target level of significance in units of standard deviation. With

JHEP10(2013)005

this optimisation the BDT classifier is found to retain 44% of the $B^0_{(s)} \to p\overline{p}$ signals while reducing the combinatorial background level by 99.6%.

The kinematic selection of the $B^0 \to K^+\pi^-$ decay is performed using individual requirements on a set of variables similar to that used for the BDT selection of the $B^0_{(s)} \to p\overline{p}$ decays, except that the cone variables are not used. This selection differs from the selection used for signal modes and follows from the synergy with ongoing LHCb analyses on two-body charmless B decays, e.g. ref. [28].

The particle identification (PID) criteria applied in addition to the $B^0_{(s)} \to p\overline{p}$ BDT classifier are also optimised via eq. 3.1. In this instance, the signal efficiencies are determined from data control samples owing to known discrepancies between data and simulation for the PID variables. Proton PID efficiencies are tabulated in bins of p, $p_{\rm T}$ and the number of tracks in the event from data control samples of $\Lambda \to p\pi^-$ decays that are selected solely using kinematic criteria. Pion and kaon efficiencies are likewise tabulated from data control samples of $D^{*+} \to D^0(\to K^-\pi^+)\,\pi^+$ decays. The kinematic distributions of the simulated decay modes are then used to determine an average PID efficiency.

Specific PID criteria are separately defined for the two signal modes and the normalisation channel. The PID efficiencies are found to be approximately 56% for the $B^0_{(s)} \to p\overline{p}$ signals and 42% for $B^0 \to K^+\pi^-$ decays.

The ratio of efficiencies of $B^0_{(s)} \to p\overline{p}$ with respect to $B^0 \to K^+\pi^-$, $\epsilon_{B^0_{(s)}\to p\overline{p}}/\epsilon_{B^0\to K^+\pi^-}$, including contributions from the detector acceptance, trigger, selection and PID, is 0.60 (0.61). After all selection criteria are applied, 45 and 58009 candidates remain in the invariant mass ranges $[5080, 5480]\,{\rm MeV}/c^2$ and $[5000, 5800]\,{\rm MeV}/c^2$ of the $p\overline{p}$ and $K^+\pi^-$ spectra, respectively.

Possible sources of background to the $p\overline{p}$ and $K^+\pi^-$ spectra are investigated using simulation samples. These include partially reconstructed backgrounds with one or more particles from the decay of the b hadron escaping detection, and two-body b-hadron decays where one or both daughters are misidentified.

4 Signal yield determination

The signal and background candidates, in both the signal and normalisation channels, are separated, after full selection, using unbinned maximum likelihood fits to the invariant mass spectra.

The $K^+\pi^-$ mass spectrum of the normalisation mode is described with a series of probability density functions (PDFs) for the various components, similarly to ref. [29]: the $B^0 \to K^+\pi^-$ signal, the $B^0_s \to \pi^+K^-$ signal, the $B^0_s \to K^+K^-$, $B^0 \to \pi^+\pi^-$ and the $\Lambda^0_b \to p\pi^-$ misidentified backgrounds, partially reconstructed backgrounds, and combinatorial background. Any contamination from other decays is treated as a source of systematic uncertainty.

Both signal distributions are modelled by the sum of two Crystal Ball (CB) functions [30] describing the high and low-mass asymmetric tails. The peak values and the widths of the two CB components are constrained to be the same. All CB tail parameters and the relative normalisation of the two CB functions are fixed to the values obtained

JHEP10(2013)005

from simulation whereas the signal peak value and width are free to vary in the fit to the $K^+\pi^-$ spectrum. The $B^0_s \to \pi^+K^-$ signal width is constrained to the fitted $B^0 \to K^+\pi^-$ width such that the ratio of the widths is identical to that obtained in simulation.

The invariant mass distributions of the misidentified $B^0_s \to K^+K^-$, $B^0 \to \pi^+\pi^-$ and $\Lambda^0_b \to p\pi^-$ backgrounds are determined from simulation and modelled with non-parametric PDFs. The fractions of these misidentified backgrounds are related to the fraction of the $B^0 \to K^+\pi^-$ signal in the data via scaling factors that take into account the relative branching fractions [1, 31], b-hadron production fractions f_q [32, 33], and relevant misidentification rates. The latter are determined from calibration data samples.

Partially reconstructed backgrounds represent decay modes that can populate the spectrum when misreconstructed as signal with one or more undetected final-state particles, possibly in conjunction with misidentifications. The shape of this distribution is determined from simulation, where each contributing mode is assigned a weight dependent on its relative branching fraction, f_q and selection efficiency. The weighted sum of these partially-reconstructed backgrounds is shown to be well modelled with the sum of two exponentially-modified Gaussian (EMG) functions

$$\mathrm{EMG}(x;\mu,\sigma,\lambda) = \frac{\lambda}{2} e^{\frac{\lambda}{2}(2x+\lambda\sigma^2-2\mu)} \cdot \mathrm{erfc}\left(\frac{x+\lambda\sigma^2-\mu}{\sqrt{2}\sigma}\right), \tag{4.1}$$

where $\mathrm{erfc(x)} = 1 - \mathrm{erf(x)}$ is the complementary error function. The signs of the variable x and parameter μ are reversed compared to the standard definition of an EMG function. The parameters defining the shape of the two EMG functions and their relative weight are determined from simulation. The component fraction of the partially-reconstructed backgrounds is obtained from the fit to the data, all other parameters being fixed from simulation. The mass distribution of the combinatorial background is found to be well described by a linear function whose gradient is determined by the fit.

The fit to the $K^+\pi^-$ spectrum, presented in figure 1, determines seven parameters, and yields $N(B^0 \to K^+\pi^-) = 24\,968 \pm 198$ signal events, where the uncertainty is statistical only.

The $p\overline{p}$ spectrum is described by PDFs for the three components: the $B^0 \to p\overline{p}$ and $B^0_s \to p\overline{p}$ signals, and the combinatorial background. In particular, any contamination from partially reconstructed backgrounds, with or without misidentified particles, is treated as a source of systematic uncertainty.

Potential sources of non-combinatorial background to the $p\overline{p}$ spectrum are two- and three-body decays of b hadrons into protons, pions and kaons, and many-body b-baryon modes partially reconstructed, with one or multiple misidentifications. It is verified from extensive simulation studies that the ensemble of specific backgrounds do not peak in the signal region but rather contribute to a smooth mass spectrum, which can be accommodated by the dominant combinatorial background contribution. The most relevant backgrounds are found to be $\Lambda^0_b \to \Lambda^+_c(\to p\overline{K}^0)\pi^-$, $\Lambda^0_b \to \overline{K}^0 p\pi^-$, $B^0 \to K^+K^-\pi^0$ and $B^0 \to \pi^+\pi^-\pi^0$ decays. Calibration data samples are exploited to determine the PID efficiencies of these decay modes, thereby confirming the suppression with respect to the

JHEP10(2013)005

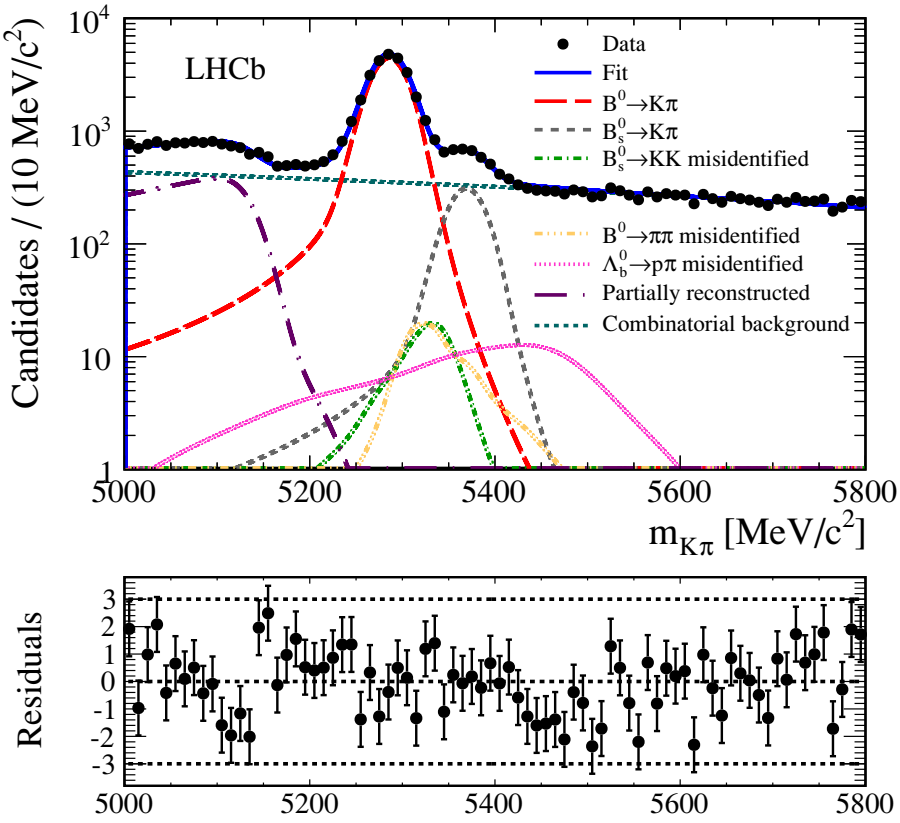

Figure 1. Invariant mass distribution of $K^+\pi^-$ candidates after full selection. The fit result (blue, solid) is superposed together with each fit model component as described in the legend. The normalised fit residual distribution is shown at the bottom.

combinatorial background by typically one or two orders of magnitude. Henceforth physics-specific backgrounds are neglected in the fit to the $p\overline{p}$ mass spectrum.

The $B^0_{(s)} \to p\overline{p}$ signal mass shapes are verified in simulation to be well described by a single Gaussian function. The widths of both Gaussian functions are assumed to be the same for $B^0 \to p\overline{p}$ and $B^0_s \to p\overline{p}$; a systematic uncertainty associated to this assumption is evaluated. They are determined from simulation with a scaling factor to account for differences in the resolution between data and simulation; the scaling factor is determined from the $B^0 \to K^+\pi^-$ data and simulation samples. The mean of the $B^0_s \to p\overline{p}$ Gaussian function is constrained according to the B^0_s–B^0 mass difference [1]. The mass distribution of the combinatorial background is described by a linear function.

The fit to the $p\overline{p}$ mass spectrum is presented in figure 2. The yields for the $B^0_{(s)} \to p\overline{p}$ signals in the full mass range are $N(B^0 \to p\overline{p}) = 11.4^{+4.3}_{-4.1}$ and $N(B^0_s \to p\overline{p}) = 5.7^{+3.5}_{-3.2}$, where the uncertainties are statistical only.

The statistical significances of the $B^0_{(s)} \to p\overline{p}$ signals are computed, using Wilks' theorem [34], from the change in the mass fit likelihood profiles when omitting the signal under scrutiny, namely $\sqrt{2\ln(L_{\rm S+B}/L_{\rm B})}$, where $L_{\rm S+B}$ and $L_{\rm B}$ are the likelihoods from the baseline fit and from the fit without the signal component, respectively. The statistical

JHEP10(2013)005

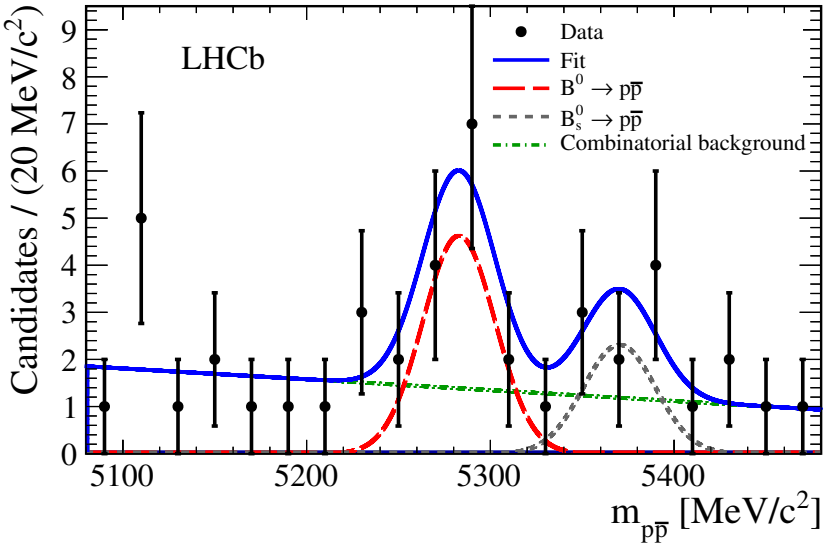

Figure 2. Invariant mass distribution of $p\bar{p}$ candidates after full selection. The fit result (blue, solid) is superposed with each fit model component: the $B^0 \to p\bar{p}$ signal (red, dashed), the $B_s^0 \to p\bar{p}$ signal (grey, dotted) and the combinatorial background (green, dot-dashed).

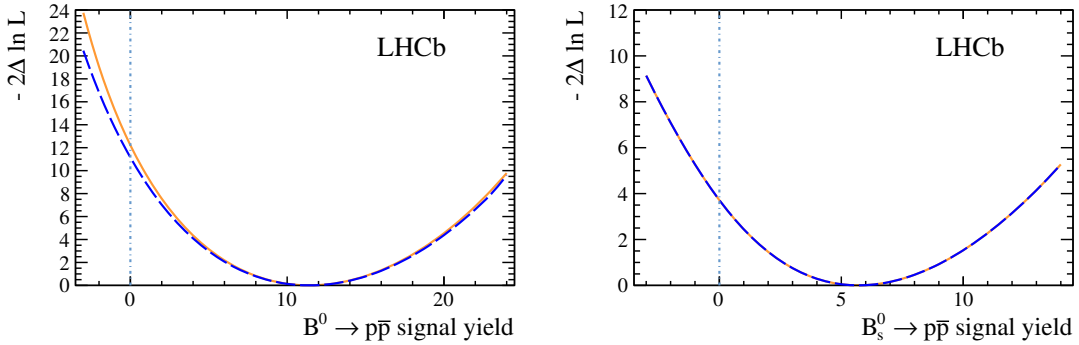

Figure 3. Negative logarithm of the profile likelihoods as a function of (left) the $B^0 \to p\bar{p}$ signal yield and (right) the $B_s^0 \to p\bar{p}$ signal yield. The orange solid curves correspond to the statistical-only profiles whereas the blue dashed curves include systematic uncertainties.

significances are $3.5\,\sigma$ and $1.9\,\sigma$ for the $B^0 \to p\bar{p}$ and $B_s^0 \to p\bar{p}$ decay modes, respectively. Each statistical-only likelihood curve is convolved with a Gaussian resolution function of width equal to the systematic uncertainty (discussed below) on the signal yield. The resulting likelihood profiles are presented in figure 3. The total signal significances are $3.3\,\sigma$ and $1.9\,\sigma$ for the $B^0 \to p\bar{p}$ and $B_s^0 \to p\bar{p}$ modes, respectively. We observe an excess of $B^0 \to p\bar{p}$ candidates with respect to background expectations; the $B_s^0 \to p\bar{p}$ signal is not considered to be statistically significant.

5 Systematic uncertainties

The sources of systematic uncertainty are minimised by performing the branching fraction measurement relative to a decay mode topologically identical to the decays of interest. They are summarised in table 1.

JHEP10(2013)005

Source	Value (%)		
	$B^0 \to p\overline{p}$	$B_s^0 \to p\overline{p}$	$B^0 \to K^+\pi^-$
$B^0 \to K^+\pi^-$ branching fraction	—	—	2.8
Trigger efficiency relative to $B^0 \to K^+\pi^-$	2.0	2.0	—
Selection efficiency relative to $B^0 \to K^+\pi^-$	8.0	8.0	—
PID efficiency	10.6	10.7	1.0
Yield from mass fit	6.8	4.6	1.6
f_s/f_d	—	7.8	—
Total	15.1	16.3	3.4

Table 1. Relative systematic uncertainties contributing to the $B^0_{(s)} \to p\overline{p}$ branching fractions. The total corresponds to the sum of all contributions added in quadrature.

The branching fraction of the normalisation channel $B^0 \to K^+\pi^-$, $\mathcal{B}(B^0 \to K^+\pi^-) = (19.55 \pm 0.54) \times 10^{-6}$ [31], is known to a precision of 2.8%, which is taken as a systematic uncertainty. For the measurement of the $B_s^0 \to p\overline{p}$ branching fraction, an extra uncertainty arises from the 7.8% uncertainty on the ratio of fragmentation fractions $f_s/f_d = 0.256 \pm 0.020$ [33].

The trigger efficiencies are assessed from simulation for all decay modes. The simulation describes well the ratio of efficiencies of the relevant modes that comprise the same number of tracks in the final state. Neglecting small p and $p_{\rm T}$ differences between the $B^0 \to p\overline{p}$ and $B_s^0 \to p\overline{p}$ modes, the ratios of $B^0 \to K^+\pi^-/B^0_{(s)} \to p\overline{p}$ trigger efficiencies should be consistent within uncertainties. The difference of about 2% observed in simulation is taken as systematic uncertainty.

The $B^0 \to K^+\pi^-$ mode is used as a proxy for the assessment of the systematic uncertainties related to the selection; $B^0 \to K^+\pi^-$ signal distributions are obtained from data, using the *sPlot* technique, for a variety of selection variables. From the level of agreement between simulation and data, a systematic uncertainty of 8% is derived for the $B^0_{(s)} \to p\overline{p}$ selection efficiencies relative to $B^0 \to K^+\pi^-$.

The PID efficiencies are determined from data control samples. The associated systematic uncertainties are estimated by repeating the procedure with simulated control samples, the uncertainties being equal to the differences observed betweeen data and simulation, scaled by the PID efficiencies estimated with the data control samples. The systematic uncertainties on the PID efficiencies are found to be 10.6%, 10.7% and 1.0% for the $B^0 \to p\overline{p}$, $B_s^0 \to p\overline{p}$ and $B^0 \to K^+\pi^-$ decay modes, respectively. The large uncertainties on the proton PID efficiencies arise from limited coverage of the proton control samples in the kinematic region of interest for the signal.

Systematic uncertainties on the fit yields arise from the limited knowledge or the choice of the mass fit models, and from the uncertainties on the values of the parameters fixed in the fits. They are investigated by studying a large number of simulated datasets,

JHEP10(2013)005

with parameters varying within their estimated uncertainties. Combining all sources of uncertainty in quadrature, the uncertainties on the $B^0 \to p\overline{p}$, $B_s^0 \to p\overline{p}$ and $B^0 \to K^+\pi^-$ yields are 6.8%, 4.6% and 1.6%, respectively.

6 Results and conclusion

The branching fractions are determined relative to the $B^0 \to K^+\pi^-$ normalisation channel according to

$$\begin{aligned}\mathcal{B}(B^0_{(s)} \to p\overline{p}) &= \frac{N(B^0_{(s)} \to p\overline{p})}{N(B^0 \to K^+\pi^-)} \cdot \frac{\epsilon_{B^0 \to K^+\pi^-}}{\epsilon_{B^0_{(s)} \to p\overline{p}}} \cdot f_d/f_{d(s)} \cdot \mathcal{B}(B^0 \to K^+\pi^-) \\ &= \alpha_{d(s)} \cdot N(B^0_{(s)} \to p\overline{p})\,, \end{aligned} \tag{6.1}$$

where $\alpha_{d(s)}$ are the single-event sensitivities equal to $(1.31 \pm 0.18) \times 10^{-9}$ and $(5.04 \pm 0.81) \times 10^{-9}$ for the $B^0 \to p\overline{p}$ and $B_s^0 \to p\overline{p}$ decay modes, respectively; their uncertainties amount to 14% and 16%, respectively.

The Feldman-Cousins (FC) frequentist method [35] is chosen for the calculation of the branching fractions. The determination of the 68.3% and 90% CL bands is performed with simulation studies relating the measured signal yields to branching fractions, and accounting for systematic uncertainties. The 68.3% and 90% CL intervals are

$$\begin{aligned}\mathcal{B}(B^0 \to p\overline{p}) &= \left(1.47\,^{+0.62\,+0.35}_{-0.51\,-0.14}\right) \times 10^{-8} \text{ at } 68.3\%\ \text{CL}\,, \\ \mathcal{B}(B^0 \to p\overline{p}) &= \left(1.47\,^{+1.09\,+0.69}_{-0.81\,-0.18}\right) \times 10^{-8} \text{ at } \quad 90\%\ \text{CL}\,, \\ \mathcal{B}(B_s^0 \to p\overline{p}) &= \left(2.84\,^{+2.03\,+0.85}_{-1.68\,-0.18}\right) \times 10^{-8} \text{ at } 68.3\%\ \text{CL}\,, \\ \mathcal{B}(B_s^0 \to p\overline{p}) &= \left(2.84\,^{+3.57\,+2.00}_{-2.12\,-0.21}\right) \times 10^{-8} \text{ at } \quad 90\%\ \text{CL}\,, \end{aligned}$$

where the first uncertainties are statistical and the second are systematic.

In summary, a search has been performed for the rare two-body charmless baryonic decays $B^0 \to p\overline{p}$ and $B_s^0 \to p\overline{p}$ using a data sample, corresponding to an integrated luminosity of 0.9 fb^{-1}, of pp collisions collected at a centre-of-mass energy of 7 TeVby the LHCb experiment. The results allow two-sided confidence limits to be placed on the branching fractions of both $B^0 \to p\overline{p}$ and $B_s^0 \to p\overline{p}$ for the first time. We observe an excess of $B^0 \to p\overline{p}$ candidates with respect to background expectations with a statistical significance of $3.3\,\sigma$. This is the first evidence for a two-body charmless baryonic B^0 decay. No significant $B_s^0 \to p\overline{p}$ signal is observed and the present result improves the previous bound by three orders of magnitude.

The measured $B^0 \to p\overline{p}$ branching fraction is incompatible with all published theoretical predictions by one to two orders of magnitude and motivates new and more precise theoretical calculations of two-body charmless baryonic B decays. An improved experimental search for these decay modes at LHCb with the full 2011 and 2012 dataset will help to clarify the situation, in particular for the $B_s^0 \to p\overline{p}$ mode.

JHEP10(2013)005

Acknowledgments

We express our gratitude to our colleagues in the CERN accelerator departments for the excellent performance of the LHC. We thank the technical and administrative staff at the LHCb institutes. We acknowledge support from CERN and from the national agencies: CAPES, CNPq, FAPERJ and FINEP (Brazil); NSFC (China); CNRS/IN2P3 and Region Auvergne (France); BMBF, DFG, HGF and MPG (Germany); SFI (Ireland); INFN (Italy); FOM and NWO (The Netherlands); SCSR (Poland); MEN/IFA (Romania); MinES, Rosatom, RFBR and NRC "Kurchatov Institute" (Russia); MinECo, XuntaGal and GENCAT (Spain); SNSF and SER (Switzerland); NAS Ukraine (Ukraine); STFC (United Kingdom); NSF (USA). We also acknowledge the support received from the ERC under FP7. The Tier1 computing centres are supported by IN2P3 (France), KIT and BMBF (Germany), INFN (Italy), NWO and SURF (The Netherlands), PIC (Spain), GridPP (United Kingdom). We are thankful for the computing resources put at our disposal by Yandex LLC (Russia), as well as to the communities behind the multiple open source software packages that we depend on.

References

[1] Particle Data Group collaboration, J. Beringer et al., *Review of particle physics*, *Phys. Rev.* **D 86** (2012) 010001 [INSPIRE].

[2] ALEPH collaboration, D. Buskulic et al., *Observation of charmless hadronic b decays*, *Phys. Lett.* **B 384** (1996) 471 [INSPIRE].

[3] CLEO collaboration, T. Coan et al., *Search for exclusive rare baryonic decays of B mesons*, *Phys. Rev.* **D 59** (1999) 111101 [hep-ex/9810043] [INSPIRE].

[4] BaBar collaboration, B. Aubert et al., *Search for the decay $B^0 \to p\bar{p}$*, *Phys. Rev.* **D 69** (2004) 091503 [hep-ex/0403003] [INSPIRE].

[5] BELLE collaboration, Y.-T. Tsai et al., *Search for $B^0 \to p\bar{p}$, $\Lambda\bar{\Lambda}$ and $B^+ \to p\bar{\Lambda}$ at Belle*, *Phys. Rev.* **D 75** (2007) 111101 [hep-ex/0703048] [INSPIRE].

[6] LHCb collaboration, *Studies of the decays $B^+ \to p\bar{p}h^+$ and observation of $B^+ \to \bar{\Lambda}(1520)p$*, *Phys. Rev. D 88,* **052015** (2013) [arXiv:1307.6165] [INSPIRE].

[7] H.Y. Cheng and J.G. Smith, *Charmless hadronic B meson decays*, *Ann. Rev. Nucl. Part. Sci.* **59** (2009) 215 [arXiv:0901.4396].

[8] V. Chernyak and I. Zhitnitsky, *B meson exclusive decays into baryons*, *Nucl. Phys.* **B 345** (1990) 137 [INSPIRE].

[9] P. Ball and H.G. Dosch, *Branching ratios of exclusive decays of bottom mesons into baryon-antibaryon pairs*, *Z. Phys.* **C 51** (1991) 445.

[10] M. Jarfi et al., *Pole model of B-meson decays into baryon-antibaryon pairs*, *Phys. Rev.* **D 43** (1991) 1599 [INSPIRE].

JHEP10(2013)005

[11] M. Jarfi et al., *Relevance of baryon-antibaryon decays of B_d^0, $\bar{B}_d^0$ in tests of CP violation*, *Phys. Lett.* **B 237** (1990) 513 [INSPIRE].

[12] H.-Y. Cheng and K.-C. Yang, *Charmless exclusive baryonic B decays*, *Phys. Rev.* **D 66** (2002) 014020 [hep-ph/0112245] [INSPIRE].

[13] LHCb collaboration, *The LHCb detector at the LHC*, 2008 *JINST* **3** S08005 [INSPIRE].

[14] M. Adinolfi et al., *Performance of the LHCb RICH detector at the LHC*, *Eur. Phys. J.* **C 73** (2013) 2431 [arXiv:1211.6759] [INSPIRE].

[15] A.A. J. Alves et al., *Performance of the LHCb muon system*, 2013 *JINST* **8** P02022 [arXiv:1211.1346] [INSPIRE].

[16] R. Aaij et al., *The LHCb trigger and its performance in 2011*, 2013 *JINST* **8** P04022 [arXiv:1211.3055] [INSPIRE].

[17] V.V. Gligorov and M. Williams, *Efficient, reliable and fast high-level triggering using a bonsai boosted decision tree*, 2013 *JINST* **8** P02013 [arXiv:1210.6861] [INSPIRE].

[18] T. Sjöstrand, S. Mrenna and P.Z. Skands, *PYTHIA 6.4 physics and manual*, *JHEP* **05** (2006) 026 [hep-ph/0603175] [INSPIRE].

[19] I. Belyaev et al., *Handling of the generation of primary events in* Gauss*, the LHCb simulation framework*, *IEEE Nucl. Sci. Symp. Conf. Rec.* (2010) 1155.

[20] D.J. Lange, *The EvtGen particle decay simulation package*, *Nucl. Instrum. Meth.* **A 462** (2001) 152 [INSPIRE].

[21] P. Golonka and Z. Was, *PHOTOS Monte Carlo: a precision tool for QED corrections in Z and W decays*, *Eur. Phys. J.* **C 45** (2006) 97 [hep-ph/0506026] [INSPIRE].

[22] GEANT4 collaboration, J. Allison et al., *GEANT4 developments and applications*, *IEEE Trans. Nucl. Sci.* **53** (2006) 270.

[23] GEANT4 collaboration, S. Agostinelli et al., *GEANT4: a simulation toolkit*, *Nucl. Instrum. Meth.* **A 506** (2003) 250 [INSPIRE].

[24] M. Clemencic et al., *The LHCb simulation application, GAUSS: design, evolution and experience*, *J. Phys. Conf. Ser.* **331** (2011) 032023 [INSPIRE].

[25] L. Breiman, J.H. Friedman, R.A. Olshen and C.J. Stone, *Classification and regression trees*, Wadsworth international group, Belmont, California U.S.A. (1984).

[26] M. Pivk and F.R. Le Diberder, *SPlot: a statistical tool to unfold data distributions*, *Nucl. Instrum. Meth.* **A 555** (2005) 356 [physics/0402083] [INSPIRE].

[27] G. Punzi, *Sensitivity of searches for new signals and its optimization*, *eConf* **C 030908** (2003) MODT002 [physics/0308063] [INSPIRE].

[28] LHCb collaboration, *Measurement of the effective $B_s^0 \to K^+K^-$ lifetime*, *Phys. Lett.* **B 716** (2012) 393 [arXiv:1207.5993] [INSPIRE].

[29] LHCb collaboration, *First observation of CP violation in the decays of B_s^0 mesons*, *Phys. Rev. Lett.* **110** (2013) 221601 [arXiv:1304.6173] [INSPIRE].

[30] T. Skwarnicki, *A study of the radiative cascade transitions between the Υ' and Υ resonances*, Ph.D. thesis, Institute of Nuclear Physics, Krakow, Poland (1986), DESY-F31-86-02.

JHEP10(2013)005

[31] Heavy Flavor Averaging Group collaboration, *Averages of b-hadron, c-hadron and τ-lepton properties as of early 2012*, arXiv:1207.1158 [INSPIRE]; updated results and plots available at http://www.slac.stanford.edu/xorg/hfag/.

[32] LHCb collaboration, *Measurement of b-hadron production fractions in* 7 TeV *pp collisions*, *Phys. Rev.* **D 85** (2012) 032008 [arXiv:1111.2357] [INSPIRE].

[33] LHCb collaboration, *Measurement of the fragmentation fraction ratio f_s/f_d and its dependence on B meson kinematics*, *JHEP* **04** (2013) 001 [arXiv:1301.5286] [INSPIRE].

[34] S.S. Wilks, *The large-sample distribution of the likelihood ratio for testing composite hypotheses*, *Ann. Math. Stat.* (1938) 60.

[35] G.J. Feldman and R.D. Cousins, *A unified approach to the classical statistical analysis of small signals*, *Phys. Rev.* **D 57** (1998) 3873 [physics/9711021] [INSPIRE].

JHEP10(2013)005

The LHCb collaboration

R. Aaij[40], B. Adeva[36], M. Adinolfi[45], C. Adrover[6], A. Affolder[51], Z. Ajaltouni[5], J. Albrecht[9], F. Alessio[37], M. Alexander[50], S. Ali[40], G. Alkhazov[29], P. Alvarez Cartelle[36], A.A. Alves Jr[24,37], S. Amato[2], S. Amerio[21], Y. Amhis[7], L. Anderlini[17,f], J. Anderson[39], R. Andreassen[56], J.E. Andrews[57], R.B. Appleby[53], O. Aquines Gutierrez[10], F. Archilli[18], A. Artamonov[34], M. Artuso[58], E. Aslanides[6], G. Auriemma[24,m], M. Baalouch[5], S. Bachmann[11], J.J. Back[47], C. Baesso[59], V. Balagura[30], W. Baldini[16], R.J. Barlow[53], C. Barschel[37], S. Barsuk[7], W. Barter[46], Th. Bauer[40], A. Bay[38], J. Beddow[50], F. Bedeschi[22], I. Bediaga[1], S. Belogurov[30], K. Belous[34], I. Belyaev[30], E. Ben-Haim[8], G. Bencivenni[18], S. Benson[49], J. Benton[45], A. Berezhnoy[31], R. Bernet[39], M.-O. Bettler[46], M. van Beuzekom[40], A. Bien[11], S. Bifani[44], T. Bird[53], A. Bizzeti[17,h], P.M. Bjørnstad[53], T. Blake[37], F. Blanc[38], J. Blouw[11], S. Blusk[58], V. Bocci[24], A. Bondar[33], N. Bondar[29], W. Bonivento[15], S. Borghi[53], A. Borgia[58], T.J.V. Bowcock[51], E. Bowen[39], C. Bozzi[16], T. Brambach[9], J. van den Brand[41], J. Bressieux[38], D. Brett[53], M. Britsch[10], T. Britton[58], N.H. Brook[45], H. Brown[51], I. Burducea[28], A. Bursche[39], G. Busetto[21,q], J. Buytaert[37], S. Cadeddu[15], O. Callot[7], M. Calvi[20,j], M. Calvo Gomez[35,n], A. Camboni[35], P. Campana[18,37], D. Campora Perez[37], A. Carbone[14,c], G. Carboni[23,k], R. Cardinale[19,i], A. Cardini[15], H. Carranza-Mejia[49], L. Carson[52], K. Carvalho Akiba[2], G. Casse[51], L. Castillo Garcia[37], M. Cattaneo[37], Ch. Cauet[9], R. Cenci[57], M. Charles[54], Ph. Charpentier[37], P. Chen[3,38], N. Chiapolini[39], M. Chrzaszcz[25], K. Ciba[37], X. Cid Vidal[37], G. Ciezarek[52], P.E.L. Clarke[49], M. Clemencic[37], H.V. Cliff[46], J. Closier[37], C. Coca[28], V. Coco[40], J. Cogan[6], E. Cogneras[5], P. Collins[37], A. Comerma-Montells[35], A. Contu[15,37], A. Cook[45], M. Coombes[45], S. Coquereau[8], G. Corti[37], B. Couturier[37], G.A. Cowan[49], E. Cowie[45], D.C. Craik[47], S. Cunliffe[52], R. Currie[49], C. D'Ambrosio[37], P. David[8], P.N.Y. David[40], A. Davis[56], I. De Bonis[4], K. De Bruyn[40], S. De Capua[53], M. De Cian[11], J.M. De Miranda[1], L. De Paula[2], W. De Silva[56], P. De Simone[18], D. Decamp[4], M. Deckenhoff[9], L. Del Buono[8], N. Déléage[4], D. Derkach[54], O. Deschamps[5], F. Dettori[41], A. Di Canto[11], H. Dijkstra[37], M. Dogaru[28], S. Donleavy[51], F. Dordei[11], A. Dosil Suárez[36], D. Dossett[47], A. Dovbnya[42], F. Dupertuis[38], P. Durante[37], R. Dzhelyadin[34], A. Dziurda[25], A. Dzyuba[29], S. Easo[48], U. Egede[52], V. Egorychev[30], S. Eidelman[33], D. van Eijk[40], S. Eisenhardt[49], U. Eitschberger[9], R. Ekelhof[9], L. Eklund[50,37], I. El Rifai[5], Ch. Elsasser[39], A. Falabella[14,e], C. Färber[11], G. Fardell[49], C. Farinelli[40], S. Farry[51], D. Ferguson[49], V. Fernandez Albor[36], F. Ferreira Rodrigues[1], M. Ferro-Luzzi[37], S. Filippov[32], M. Fiore[16], C. Fitzpatrick[37], M. Fontana[10], F. Fontanelli[19,i], R. Forty[37], O. Francisco[2], M. Frank[37], C. Frei[37], M. Frosini[17,f], S. Furcas[20], E. Furfaro[23,k], A. Gallas Torreira[36], D. Galli[14,c], M. Gandelman[2], P. Gandini[58], Y. Gao[3], J. Garofoli[58], P. Garosi[53], J. Garra Tico[46], L. Garrido[35], C. Gaspar[37], R. Gauld[54], E. Gersabeck[11], M. Gersabeck[53], T. Gershon[47,37], Ph. Ghez[4], V. Gibson[46], L. Giubega[28], V.V. Gligorov[37], C. Göbel[59], D. Golubkov[30], A. Golutvin[52,30,37], A. Gomes[2], P. Gorbounov[30,37], H. Gordon[37], C. Gotti[20], M. Grabalosa Gándara[5], R. Graciani Diaz[35], L.A. Granado Cardoso[37], E. Graugés[35], G. Graziani[17], A. Grecu[28], E. Greening[54], S. Gregson[46], P. Griffith[44], O. Grünberg[60], B. Gui[58], E. Gushchin[32], Yu. Guz[34,37], T. Gys[37], C. Hadjivasiliou[58], G. Haefeli[38], C. Haen[37], S.C. Haines[46], S. Hall[52], B. Hamilton[57], T. Hampson[45], S. Hansmann-Menzemer[11], N. Harnew[54], S.T. Harnew[45], J. Harrison[53], T. Hartmann[60], J. He[37], T. Head[37], V. Heijne[40], K. Hennessy[51], P. Henrard[5], J.A. Hernando Morata[36], E. van Herwijnen[37], M. Hess[60], A. Hicheur[1], E. Hicks[51], D. Hill[54], M. Hoballah[5], C. Hombach[53], P. Hopchev[4], W. Hulsbergen[40], P. Hunt[54], T. Huse[51], N. Hussain[54], D. Hutchcroft[51], D. Hynds[50], V. Iakovenko[43], M. Idzik[26], P. Ilten[12], R. Jacobsson[37], A. Jaeger[11], E. Jans[40], P. Jaton[38], A. Jawahery[57], F. Jing[3], M. John[54], D. Johnson[54], C.R. Jones[46], C. Joram[37], B. Jost[37], M. Kaballo[9], S. Kandybei[42], W. Kanso[6], M. Karacson[37], T.M. Karbach[37],

JHEP10(2013)005

I.R. Kenyon[44], T. Ketel[41], A. Keune[38], B. Khanji[20], O. Kochebina[7], I. Komarov[38], R.F. Koopman[41], P. Koppenburg[40], M. Korolev[31], A. Kozlinskiy[40], L. Kravchuk[32], K. Kreplin[11], M. Kreps[47], G. Krocker[11], P. Krokovny[33], F. Kruse[9], M. Kucharczyk[20,25,j], V. Kudryavtsev[33], K. Kurek[27], T. Kvaratskheliya[30,37], V.N. La Thi[38], D. Lacarrere[37], G. Lafferty[53], A. Lai[15], D. Lambert[49], R.W. Lambert[41], E. Lanciotti[37], G. Lanfranchi[18], C. Langenbruch[37], T. Latham[47], C. Lazzeroni[44], R. Le Gac[6], J. van Leerdam[40], J.-P. Lees[4], R. Lefèvre[5], A. Leflat[31], J. Lefrançois[7], S. Leo[22], O. Leroy[6], T. Lesiak[25], B. Leverington[11], Y. Li[3], L. Li Gioi[5], M. Liles[51], R. Lindner[37], C. Linn[11], B. Liu[3], G. Liu[37], S. Lohn[37], I. Longstaff[50], J.H. Lopes[2], N. Lopez-March[38], H. Lu[3], D. Lucchesi[21,q], J. Luisier[38], H. Luo[49], F. Machefert[7], I.V. Machikhiliyan[4,30], F. Maciuc[28], O. Maev[29,37], S. Malde[54], G. Manca[15,d], G. Mancinelli[6], J. Maratas[5], U. Marconi[14], P. Marino[22,s], R. Märki[38], J. Marks[11], G. Martellotti[24], A. Martens[8], A. Martín Sánchez[7], M. Martinelli[40], D. Martinez Santos[41], D. Martins Tostes[2], A. Martynov[31], A. Massafferri[1], R. Matev[37], Z. Mathe[37], C. Matteuzzi[20], E. Maurice[6], A. Mazurov[16,32,37,e], J. McCarthy[44], A. McNab[53], R. McNulty[12], B. McSkelly[51], B. Meadows[56,54], F. Meier[9], M. Meissner[11], M. Merk[40], D.A. Milanes[8], M.-N. Minard[4], J. Molina Rodriguez[59], S. Monteil[5], D. Moran[53], P. Morawski[25], A. Mordà[6], M.J. Morello[22,s], R. Mountain[58], I. Mous[40], F. Muheim[49], K. Müller[39], R. Muresan[28], B. Muryn[26], B. Muster[38], P. Naik[45], T. Nakada[38], R. Nandakumar[48], I. Nasteva[1], M. Needham[49], S. Neubert[37], N. Neufeld[37], A.D. Nguyen[38], T.D. Nguyen[38], C. Nguyen-Mau[38,o], M. Nicol[7], V. Niess[5], R. Niet[9], N. Nikitin[31], T. Nikodem[11], A. Nomerotski[54], A. Novoselov[34], A. Oblakowska-Mucha[26], V. Obraztsov[34], S. Oggero[40], S. Ogilvy[50], O. Okhrimenko[43], R. Oldeman[15,d], M. Orlandea[28], J.M. Otalora Goicochea[2], P. Owen[52], A. Oyanguren[35], B.K. Pal[58], A. Palano[13,b], T. Palczewski[27], M. Palutan[18], J. Panman[37], A. Papanestis[48], M. Pappagallo[50], C. Parkes[53], C.J. Parkinson[52], G. Passaleva[17], G.D. Patel[51], M. Patel[52], G.N. Patrick[48], C. Patrignani[19,i], C. Pavel-Nicorescu[28], A. Pazos Alvarez[36], A. Pellegrino[40], G. Penso[24,l], M. Pepe Altarelli[37], S. Perazzini[14,c], E. Perez Trigo[36], A. Pérez-Calero Yzquierdo[35], P. Perret[5], M. Perrin-Terrin[6], L. Pescatore[44], E. Pesen[61], K. Petridis[52], A. Petrolini[19,i], A. Phan[58], E. Picatoste Olloqui[35], B. Pietrzyk[4], T. Pilař[47], D. Pinci[24], S. Playfer[49], M. Plo Casasus[36], F. Polci[8], G. Polok[25], A. Poluektov[47,33], E. Polycarpo[2], A. Popov[34], D. Popov[10], B. Popovici[28], C. Potterat[35], A. Powell[54], J. Prisciandaro[38], A. Pritchard[51], C. Prouve[7], V. Pugatch[43], A. Puig Navarro[38], G. Punzi[22,r], W. Qian[4], J.H. Rademacker[45], B. Rakotomiaramanana[38], M.S. Rangel[2], I. Raniuk[42], N. Rauschmayr[37], G. Raven[41], S. Redford[54], M.M. Reid[47], A.C. dos Reis[1], S. Ricciardi[48], A. Richards[52], K. Rinnert[51], V. Rives Molina[35], D.A. Roa Romero[5], P. Robbe[7], D.A. Roberts[57], E. Rodrigues[53], P. Rodriguez Perez[36], S. Roiser[37], V. Romanovsky[34], A. Romero Vidal[36], J. Rouvinet[38], T. Ruf[37], F. Ruffini[22], H. Ruiz[35], P. Ruiz Valls[35], G. Sabatino[24,k], J.J. Saborido Silva[36], N. Sagidova[29], P. Sail[50], B. Saitta[15,d], V. Salustino Guimaraes[2], B. Sanmartin Sedes[36], M. Sannino[19,i], R. Santacesaria[24], C. Santamarina Rios[36], E. Santovetti[23,k], M. Sapunov[6], A. Sarti[18,l], C. Satriano[24,m], A. Satta[23], M. Savrie[16,e], D. Savrina[30,31], P. Schaack[52], M. Schiller[41], H. Schindler[37], M. Schlupp[9], M. Schmelling[10], B. Schmidt[37], O. Schneider[38], A. Schopper[37], M.-H. Schune[7], R. Schwemmer[37], B. Sciascia[18], A. Sciubba[24], M. Seco[36], A. Semennikov[30], K. Senderowska[26], I. Sepp[52], N. Serra[39], J. Serrano[6], P. Seyfert[11], M. Shapkin[34], I. Shapoval[16,42], P. Shatalov[30], Y. Shcheglov[29], T. Shears[51,37], L. Shekhtman[33], O. Shevchenko[42], V. Shevchenko[30], A. Shires[9], R. Silva Coutinho[47], M. Sirendi[46], N. Skidmore[45], T. Skwarnicki[58], N.A. Smith[51], E. Smith[54,48], J. Smith[46], M. Smith[53], M.D. Sokoloff[56], F.J.P. Soler[50], F. Soomro[38], D. Souza[45], B. Souza De Paula[2], B. Spaan[9], A. Sparkes[49], P. Spradlin[50], F. Stagni[37], S. Stahl[11], O. Steinkamp[39], S. Stevenson[54], S. Stoica[28], S. Stone[58], B. Storaci[39], M. Straticiuc[28], U. Straumann[39], V.K. Subbiah[37], L. Sun[56], S. Swientek[9], V. Syropoulos[41], M. Szczekowski[27], P. Szczypka[38,37], T. Szumlak[26], S. T'Jampens[4], M. Teklishyn[7], E. Teodorescu[28], F. Teubert[37],

JHEP10(2013)005

C. Thomas[54], E. Thomas[37], J. van Tilburg[11], V. Tisserand[4], M. Tobin[38], S. Tolk[41], D. Tonelli[37], S. Topp-Joergensen[54], N. Torr[54], E. Tournefier[4,52], S. Tourneur[38], M.T. Tran[38], M. Tresch[39], A. Tsaregorodtsev[6], P. Tsopelas[40], N. Tuning[40], M. Ubeda Garcia[37], A. Ukleja[27], D. Urner[53], A. Ustyuzhanin[52,p], U. Uwer[11], V. Vagnoni[14], G. Valenti[14], A. Vallier[7], M. Van Dijk[45], R. Vazquez Gomez[18], P. Vazquez Regueiro[36], C. Vázquez Sierra[36], S. Vecchi[16], J.J. Velthuis[45], M. Veltri[17,g], G. Veneziano[38], M. Vesterinen[37], B. Viaud[7], D. Vieira[2], X. Vilasis-Cardona[35,n], A. Vollhardt[39], D. Volyanskyy[10], D. Voong[45], A. Vorobyev[29], V. Vorobyev[33], C. Voß[60], H. Voss[10], R. Waldi[60], C. Wallace[47], R. Wallace[12], S. Wandernoth[11], J. Wang[58], D.R. Ward[46], N.K. Watson[44], A.D. Webber[53], D. Websdale[52], M. Whitehead[47], J. Wicht[37], J. Wiechczynski[25], D. Wiedner[11], L. Wiggers[40], G. Wilkinson[54], M.P. Williams[47,48], M. Williams[55], F.F. Wilson[48], J. Wimberley[57], J. Wishahi[9], W. Wislicki[27], M. Witek[25], S.A. Wotton[46], S. Wright[46], S. Wu[3], K. Wyllie[37], Y. Xie[49,37], Z. Xing[58], Z. Yang[3], R. Young[49], X. Yuan[3], O. Yushchenko[34], M. Zangoli[14], M. Zavertyaev[10,a], F. Zhang[3], L. Zhang[58], W.C. Zhang[12], Y. Zhang[3], A. Zhelezov[11], A. Zhokhov[30], L. Zhong[3], A. Zvyagin[37]

[1] *Centro Brasileiro de Pesquisas Físicas (CBPF), Rio de Janeiro, Brazil*
[2] *Universidade Federal do Rio de Janeiro (UFRJ), Rio de Janeiro, Brazil*
[3] *Center for High Energy Physics, Tsinghua University, Beijing, China*
[4] *LAPP, Université de Savoie, CNRS/IN2P3, Annecy-Le-Vieux, France*
[5] *Clermont Université, Université Blaise Pascal, CNRS/IN2P3, LPC, Clermont-Ferrand, France*
[6] *CPPM, Aix-Marseille Université, CNRS/IN2P3, Marseille, France*
[7] *LAL, Université Paris-Sud, CNRS/IN2P3, Orsay, France*
[8] *LPNHE, Université Pierre et Marie Curie, Université Paris Diderot, CNRS/IN2P3, Paris, France*
[9] *Fakultät Physik, Technische Universität Dortmund, Dortmund, Germany*
[10] *Max-Planck-Institut für Kernphysik (MPIK), Heidelberg, Germany*
[11] *Physikalisches Institut, Ruprecht-Karls-Universität Heidelberg, Heidelberg, Germany*
[12] *School of Physics, University College Dublin, Dublin, Ireland*
[13] *Sezione INFN di Bari, Bari, Italy*
[14] *Sezione INFN di Bologna, Bologna, Italy*
[15] *Sezione INFN di Cagliari, Cagliari, Italy*
[16] *Sezione INFN di Ferrara, Ferrara, Italy*
[17] *Sezione INFN di Firenze, Firenze, Italy*
[18] *Laboratori Nazionali dell'INFN di Frascati, Frascati, Italy*
[19] *Sezione INFN di Genova, Genova, Italy*
[20] *Sezione INFN di Milano Bicocca, Milano, Italy*
[21] *Sezione INFN di Padova, Padova, Italy*
[22] *Sezione INFN di Pisa, Pisa, Italy*
[23] *Sezione INFN di Roma Tor Vergata, Roma, Italy*
[24] *Sezione INFN di Roma La Sapienza, Roma, Italy*
[25] *Henryk Niewodniczanski Institute of Nuclear Physics Polish Academy of Sciences, Kraków, Poland*
[26] *AGH - University of Science and Technology, Faculty of Physics and Applied Computer Science, Kraków, Poland*
[27] *National Center for Nuclear Research (NCBJ), Warsaw, Poland*
[28] *Horia Hulubei National Institute of Physics and Nuclear Engineering, Bucharest-Magurele, Romania*
[29] *Petersburg Nuclear Physics Institute (PNPI), Gatchina, Russia*
[30] *Institute of Theoretical and Experimental Physics (ITEP), Moscow, Russia*
[31] *Institute of Nuclear Physics, Moscow State University (SINP MSU), Moscow, Russia*
[32] *Institute for Nuclear Research of the Russian Academy of Sciences (INR RAN), Moscow, Russia*
[33] *Budker Institute of Nuclear Physics (SB RAS) and Novosibirsk State University, Novosibirsk, Russia*

JHEP10(2013)005

[34] Institute for High Energy Physics (IHEP), Protvino, Russia
[35] Universitat de Barcelona, Barcelona, Spain
[36] Universidad de Santiago de Compostela, Santiago de Compostela, Spain
[37] European Organization for Nuclear Research (CERN), Geneva, Switzerland
[38] Ecole Polytechnique Fédérale de Lausanne (EPFL), Lausanne, Switzerland
[39] Physik-Institut, Universität Zürich, Zürich, Switzerland
[40] Nikhef National Institute for Subatomic Physics, Amsterdam, The Netherlands
[41] Nikhef National Institute for Subatomic Physics and VU University Amsterdam, Amsterdam, The Netherlands
[42] NSC Kharkiv Institute of Physics and Technology (NSC KIPT), Kharkiv, Ukraine
[43] Institute for Nuclear Research of the National Academy of Sciences (KINR), Kyiv, Ukraine
[44] University of Birmingham, Birmingham, United Kingdom
[45] H.H. Wills Physics Laboratory, University of Bristol, Bristol, United Kingdom
[46] Cavendish Laboratory, University of Cambridge, Cambridge, United Kingdom
[47] Department of Physics, University of Warwick, Coventry, United Kingdom
[48] STFC Rutherford Appleton Laboratory, Didcot, United Kingdom
[49] School of Physics and Astronomy, University of Edinburgh, Edinburgh, United Kingdom
[50] School of Physics and Astronomy, University of Glasgow, Glasgow, United Kingdom
[51] Oliver Lodge Laboratory, University of Liverpool, Liverpool, United Kingdom
[52] Imperial College London, London, United Kingdom
[53] School of Physics and Astronomy, University of Manchester, Manchester, United Kingdom
[54] Department of Physics, University of Oxford, Oxford, United Kingdom
[55] Massachusetts Institute of Technology, Cambridge, MA, United States
[56] University of Cincinnati, Cincinnati, OH, United States
[57] University of Maryland, College Park, MD, United States
[58] Syracuse University, Syracuse, NY, United States
[59] Pontifícia Universidade Católica do Rio de Janeiro (PUC-Rio), Rio de Janeiro, Brazil, associated to[2]
[60] Institut für Physik, Universität Rostock, Rostock, Germany, associated to[11]
[61] Celal Bayar University, Manisa, Turkey, associated to[37]

[a] P.N. Lebedev Physical Institute, Russian Academy of Science (LPI RAS), Moscow, Russia
[b] Università di Bari, Bari, Italy
[c] Università di Bologna, Bologna, Italy
[d] Università di Cagliari, Cagliari, Italy
[e] Università di Ferrara, Ferrara, Italy
[f] Università di Firenze, Firenze, Italy
[g] Università di Urbino, Urbino, Italy
[h] Università di Modena e Reggio Emilia, Modena, Italy
[i] Università di Genova, Genova, Italy
[j] Università di Milano Bicocca, Milano, Italy
[k] Università di Roma Tor Vergata, Roma, Italy
[l] Università di Roma La Sapienza, Roma, Italy
[m] Università della Basilicata, Potenza, Italy
[n] LIFAELS, La Salle, Universitat Ramon Llull, Barcelona, Spain
[o] Hanoi University of Science, Hanoi, Viet Nam
[p] Institute of Physics and Technology, Moscow, Russia
[q] Università di Padova, Padova, Italy
[r] Università di Pisa, Pisa, Italy
[s] Scuola Normale Superiore, Pisa, Italy

JHEP10(2013)005